


**CO<sub>2</sub> Reduction Hot Paper**
How to cite: *Angew. Chem. Int. Ed.* **2021**, 60, 8983–8989

International Edition: doi.org/10.1002/anie.202016710

German Edition: doi.org/10.1002/ange.202016710

# Robust Biological Hydrogen-Bonded Organic Framework with Post-Functionalized Rhenium(I) Sites for Efficient Heterogeneous Visible-Light-Driven CO<sub>2</sub> Reduction

Baoqiu Yu, Lianjie Li, Shanshan Liu, Hailong Wang,\* Heyuan Liu, Chenxiang Lin, Chao Liu, Hui Wu, Wei Zhou, Xiyu Li, Tianyu Wang, Banglin Chen,\* and Jianzhuang Jiang\*

**Abstract:** A robust 2,2'-bipyridine (bpy)-derived biological hydrogen-bonded framework (HOF-25) has been realized depending on guanine-quadruplex with the assistance of  $\pi$ - $\pi$  interaction, which reacts with  $\text{Re}(\text{CO})_5\text{Cl}$  to give a post-functionalized HOF-25-Re. X-ray absorption fine structure spectroscopic study on HOF-25-Re confirms the covalent attachment of  $\text{Re}(\text{bpy})(\text{CO})_3\text{Cl}$  segments to this HOF. Robust and recycled HOF-25-Re bearing photocatalytic  $\text{Re}(\text{bpy})(\text{CO})_3\text{Cl}$  centers displays good heterogeneous catalytic activity towards carbon dioxide photoreduction in the presence of  $[\text{Ru}(\text{bpy})_3]\text{Cl}_2$  and triisopropanolamine in  $\text{CH}_3\text{CN}$  under visible-light irradiation, with both high CO production rate of  $1448 \mu\text{mol g}^{-1} \text{h}^{-1}$  and high selectivity of 93%. Under the same conditions, the experimental turnover number of HOF-25-Re (50) is about 8 times as that of the homogeneous control  $\text{Re}(\text{bpy})(\text{CO})_3\text{Cl}$ . The sustainably regenerated HOF-25-Re via crystallization and post-modification processes shows recovered photocatalytic performance.

## Introduction

Carbon dioxide fixation and reduction is a promising approach to address the increasing energy crisis and global warming by outputting sustainable carbon fuels/chemicals

and mitigating anthropogenic CO<sub>2</sub> emission simultaneously.<sup>[1]</sup> In the study of CO<sub>2</sub> conversion applicability, various crystalline porous materials including zeolites,<sup>[2]</sup> metal-organic frameworks (MOFs),<sup>[1a,3]</sup> and covalent organic frameworks (COFs),<sup>[1b,4]</sup> have been estimated to transform carbon dioxide molecules using organic reaction, hydrogenation, photocatalytic reduction, and electrocatalytic reduction. Compared with amorphous porous materials, the well-defined structures of these crystalline porous species are helpful in correlating the structure with CO<sub>2</sub> conversion property from the atomic and molecular perspective.

As another kind of crystalline porous materials, hydrogen-bonded organic frameworks (HOFs), which are constructed by the self-assembly of organic or metal-organic building blocks through hydrogen-bonding, have been conceptually proposed in early 1990s,<sup>[5]</sup> but only recently been paid increasingly attentions because of their uniqueness in term of their easy solution processability and simple regeneration through simple recrystallization as well as their versatile applications including gas storage,<sup>[6]</sup> small molecule separation,<sup>[7]</sup> chiral separation,<sup>[8]</sup> sensing,<sup>[9]</sup> heterogeneous catalysis,<sup>[10]</sup> and proton conduction.<sup>[11]</sup> In comparison with the coordination and covalent bond in MOFs and COFs, the instability and low-directionality of hydrogen-bonding nature in HOFs are still the stumbling block to the establishment of permanent porosity and thus the development of diverse functions for this kind of materials. Combination of directional hydrogen-bonded synthons and suitable organic skeletons, which prefer to form strong  $\pi$ - $\pi$  interactions, has been demonstrated to effectively consolidate the frameworks of HOFs.<sup>[12]</sup> Thus far, this strategy however has not yet been widely spread due to the uncontrollable  $\pi$ - $\pi$  interactions of organic skeleton. It is therefore necessary to establish new synthetic strategy for preparing robust functional HOFs and even for realizing their post-functionalization towards a much wider variety of applications.

Herein, a biological HOF (HOF-25) has been designed and afforded by hydrogen-bonded guanine-quadruplex (G-quadruplex) directing the self-assembly of a 2,2'-bipyridine (bpy)-derived building block (L) (Scheme 1 and Figure 1 a). This robust HOF is stabilized synergistically by the hydrogen-bonded G-quadruplexes and their interlayered  $\pi$ - $\pi$  interactions, showing the permanent porosity with a Brunauer-Emmett-Teller (BET) surface area of  $173 \text{ m}^2 \text{ g}^{-1}$  acquired from the 196 K CO<sub>2</sub> adsorption fitting. In addition, this HOF can tolerate the soaking in aqueous solution with pH value from 7.0 to 11.0 as well as common organic solvents as

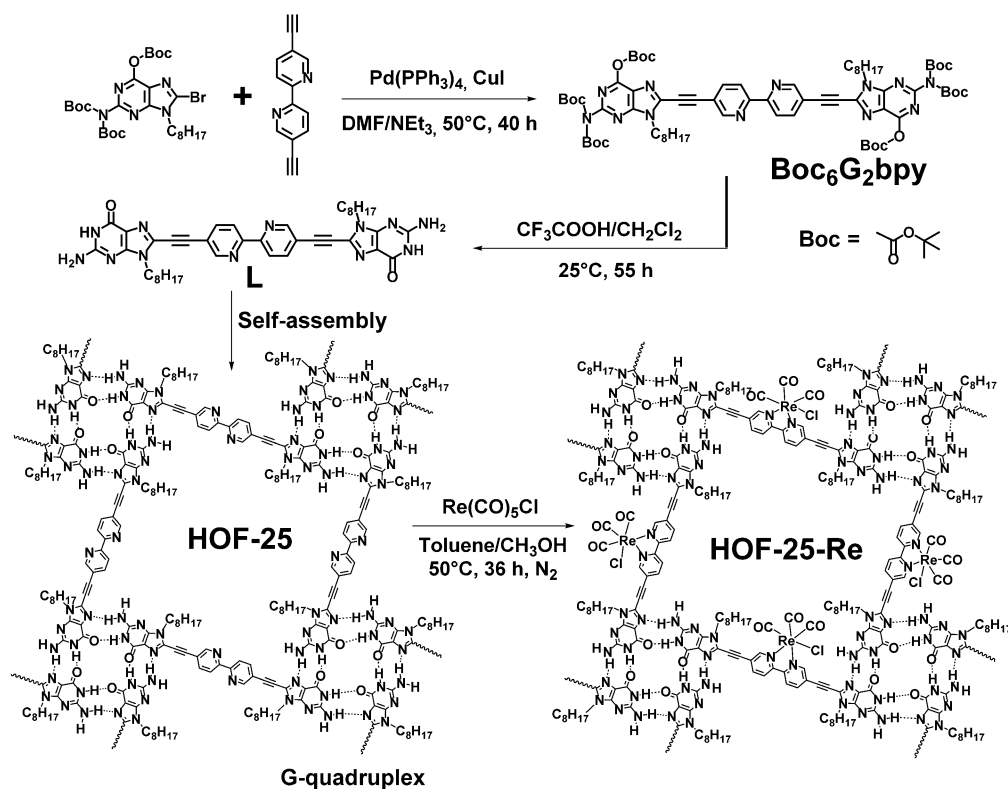
[\*] B. Yu, L. Li, Prof. H. Wang, C. Lin, C. Liu, Prof. T. Wang, Prof. J. Jiang Beijing Advanced Innovation Center for Materials Genome Engineering, Beijing Key Laboratory for Science and Application of Functional Molecular and Crystalline Materials, Department of Chemistry and Chemical Engineering, School of Chemistry and Biological Engineering, University of Science and Technology Beijing Beijing 100083 (China)  
E-mail: hlwang@ustb.edu.cn  
jianzhuang@ustb.edu.cn

Prof. B. Chen  
Department of Chemistry, University of Texas at San Antonio  
San Antonio, TX 78249-0698 (USA)  
E-mail: banglin.chen@utsa.edu

S. Liu, Dr. H. Liu, Prof. X. Li  
School of Materials Science and Engineering, China University of Petroleum (East China)  
Qingdao 266580 (China)

Dr. H. Wu, Dr. W. Zhou  
Center for Neutron Research, National Institute of Standards and Technology  
Gaithersburg, MD 20899-6102 (USA)

 Supporting information and the ORCID identification number(s) for the author(s) of this article can be found under:  
<https://doi.org/10.1002/anie.202016710>.



**Scheme 1.** Synthesis of Boc<sub>6</sub>C<sub>2</sub>bpy and Building Block (L) for the Assembly of HOF-25 and HOF-25-Re.

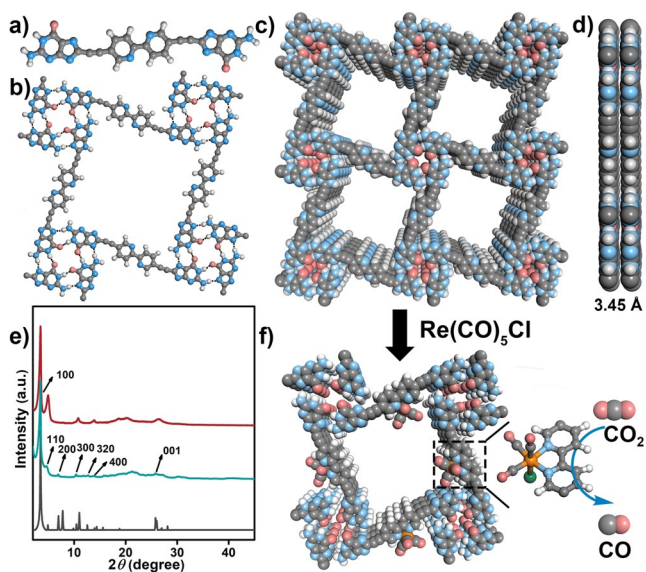


**Figure 1.** Structures of L (a), proposed G-quadruplex grid (b), and AA packing mode of HOF-25 (c and d). e) PXRD pattern comparison between activated HOF-25 (red), as-synthesized HOF-25 (cyan), and the simulated one (grey). f) A proposed structure of HOF-25-Re for carbon dioxide reduction. [Octyl chains on the guanine unit are not shown in these structures. C: grey; N: cyan; O: red; H: white; Re: yellow; Cl: green].

indicated by the powder X-ray diffraction (PXRD) analysis. The post-modification of HOF-25 with Re(CO)<sub>5</sub>Cl gives a Re-functionalized porous HOF (HOF-25-Re) with the

covalent decoration of Re(bpy)(CO)<sub>3</sub>Cl units to the hydrogen-bonded reticular framework based on the extended X-ray absorption fine structure spectroscopic (EXAFS) and PXRD studies. As a result, by adding [Ru(bpy)<sub>3</sub>]Cl<sub>2</sub>·6H<sub>2</sub>O photosensitizer in CH<sub>3</sub>CN containing triisopropanolamine (TIPA), stable and recyclable HOF-25-Re heterogeneous catalyst promotes the visible light photoreduction of carbon dioxide with a high CO production rate of 1448 μmol g<sup>-1</sup> h<sup>-1</sup> and constantly high CO selectivity of 93% for three cycles. The photocatalytic performance of overused HOF-25-Re could be recovered via a two-step treatment including crystallization and post-modification. Interestingly, the turnover number (TON) of heterogeneous HOF-25-Re (50) is obviously superior to that of the homogeneous control Re(bpy)(CO)<sub>3</sub>Cl (6) under the same photocatalytic conditions following the electron transfer from photosensitizer to photocatalyst. These results highlight the opportunity of rigid HOFs in heterogenizing molecular catalyst for diverse transformations.

## Results and Discussion

### Design and Assembly of HOF-25 and HOF-25-Re

Biological G-quadruplex moiety serves as a rigid hydrogen-bonded scaffold for the design and synthesis of various supramolecular assemblies due to its eight Hoogsteen hydrogen bonds among four guanine units.<sup>[13]</sup> In particular, the planar G-quadruplex prefers to form π-π stacking, further consolidating the hydrogen-bonded assemblies. As a result,

the guanine-decorated building blocks, which are able to pin molecular catalysts, seem to be good candidates in constructing robust porous HOFs as a new heterogenized platform. Towards detailing such a proof-of-concept, the sonogashira coupling of Boc-protected guanine derivative with 5,5'-diethynyl-2,2'-bipyridine provided Boc<sub>6</sub>G<sub>2</sub>bpy as the precursor of L (Scheme 1 and Figures S1 and S2). The biological HOF-25 was obtained by the deprotection reaction of Boc<sub>6</sub>G<sub>2</sub>bpy in a mixed solution of TFA and CH<sub>2</sub>Cl<sub>2</sub> followed by the subsequent self-assembly of L after simultaneous solvent evaporation&diffusion (Figures S3 and S4). Reaction of bpy groups in HOF-25 with Re(CO)<sub>5</sub>Cl in a solution of toluene and methanol gave HOF-25-Re with the aim to graft Re(bpy)(CO)<sub>3</sub>Cl functional sites on this HOF.

### Characterization of HOF-25

The HOF-25 structure was investigated using PXRD (Figures 1 a–e). As shown in Figure 1 e, there exists an intense diffraction peak at  $2\theta \approx 3.47^\circ$  and several relatively weak peaks at  $4.72^\circ$ ,  $6.93^\circ$ ,  $10.38^\circ$ ,  $12.75^\circ$ ,  $13.83^\circ$ , and  $25.80^\circ$  in the experimental PXRD pattern of the HOF-25 sample. Based on peak indexing, HOF-25 crystal belongs to the tetragonal system. Similar to G-quadruplex organic frameworks assembled from guanine-functionalized naphthalene diimide derivatives,<sup>[13a,b]</sup> G-quadruplex directs L to form a two-dimensional supramolecular grid with a four-connected sql net (Figures 1 a and b). As detailed in the Supporting Information, an AA-stacking structural model with space group of *P4/m* is established (Figures 1 c and d). This is supported by the Le Bail fitting on as-synthesized HOF-25 with good agreement factors  $a = b = 25.516(6) \text{ \AA}$  and  $c = 3.448(2) \text{ \AA}$ ,  $R_p = 0.0595$ ,  $R_{wp} = 0.0782$ , (Figure S5). The simulated PXRD pattern based on the present structural model is overall consistent with the experimental data. The seven diffraction peaks mentioned above correspond to (100), (110), (200), (300), (320), (400), and (001) reflections, respectively (Figure 1 e). The strong (100) diffraction and moderately strong (110) diffraction indicate a long-range order within the *ab* plane. The distance of adjacent G-quadruplex centers in the square grid is 2.54 nm. Grid-like hydrogen-bonded layers are further stacked into a three-dimensional supramolecular structure via interlayered  $\pi$ - $\pi$  interactions with the layer-layer separation of  $\approx 3.45 \text{ \AA}$  (Figures 1 c and d). Note that the octyl chains on the guanosine units are relatively “soft” and most likely disordered. Therefore, they are not included in the structural model. This is partly the reason for the difference in relative intensities between the experimental and simulated PXRD patterns. Scanning electron microscopy (SEM) photo shows the nanoscale morphology of HOF-25 (Figure 2 a). The crystalline nature of HOF-25 is verified by high resolution transmission electron microscope (HRTEM) images with clear lattice fringes, indicating the *d*-spacing of 0.4 nm (Figure 2 b).

HOF-25 shows good thermostability with the decomposed temperature higher than 400 °C (Figure S6). Powder XRD studies also reveal that the structure periodicity of pristine HOF-25 was well preserved after soaking in the aqueous

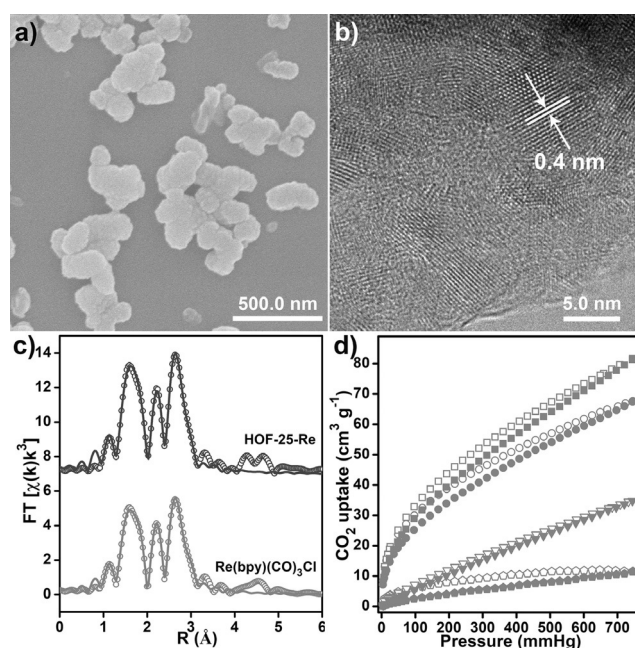


**Figure 2.** a) SEM micrograph of HOF-25. b) HRTEM micrograph of HOF-25. c) EXAFS spectroscopic data of HOF-25-Re and Re(bpy)(CO)<sub>3</sub>Cl complex in energy R-space at Re L<sub>3</sub>-edge (solid lines are fitting lines). d) CO<sub>2</sub> adsorption (solid) and desorption (hollow) curves of HOF-25 (196 K: square, 273 K: triangle) and HOF-25-Re (196 K: circle, 273 K: pentagon), respectively.

solution with pH 7.0–11.0 and common organic solvents (including acetonitrile, methanol, toluene, and acetone) in Figures S7 and S8. The robust bpy-containing HOF-25 with excellent tolerance to common solvents is the premise of post-modification and provides a new candidate to graft the molecular metal complex. In addition, the robustness of HOF-25 was also evidenced by the matched PXRD patterns between as-synthesized and activated samples obtained by degassing dichloromethane-exchanged HOF-25 at 25 °C (Figure 1 e).

### Characterization of HOF-25-Re

After the post-functionalization of HOF-25 with Re(CO)<sub>5</sub>Cl, the hydrogen-bonded reticular structure is maintained by HOF-25-Re referring to the similar PXRD pattern with the parent sample (Figures 1 f and S9). However, a slight expansion of framework is observed according to the shift of (100) diffraction due to the introduction of Re(CO)<sub>5</sub>Cl. The nanoscale morphology and crystalline nature of this HOF material were determined by the SEM and HRTEM characterizations (Figure S10a and 10b). An ICP-OES analysis indicates 1.1 wt % Re content in HOF-25-Re, corresponding to the transformation of about one-sixteenth bpy units in HOF to Re(bpy)(CO)<sub>3</sub>Cl. X-ray photoelectron spectra (XPS) of HOF-25-Re together with Re(bpy)(CO)<sub>3</sub>Cl benchmark have been collected (Figure S11), revealing the existence of C, N, O, Re, and Cl for both samples. The monovalent rhenium in HOF-25-Re is indicated by the two distinct Re 4f<sub>5/2</sub>

$2$  and Re  $4f_{7/2}$  peaks appearing at the binding energy of 44.2 and 41.9 eV (Figure S12), suggesting the graft of Re-functional sites. Despite the similar XPS peak profiles, a shift from the binding energies at 43.8&41.5 eV for Re(bpy)(CO)<sub>3</sub>Cl to 44.2&41.9 eV for HOF-25-Re is observed due possibly to the introduction of acetylene groups to the former compound, which influences the coordination field strength. In addition, the characteristic  $\nu(\text{CO})$  bands of Re(bpy)(CO)<sub>3</sub>Cl appear between 2050 and 1850 cm<sup>-1</sup> in the IR spectrum of HOF-25-Re (Figure S13).<sup>[14]</sup> These results suggest the inclusion of Re(bpy)(CO)<sub>3</sub>Cl catalytic active units in HOF-25-Re. The possible generation of rhenium nanoparticles for HOF-25-Re under the post-synthetic conditions is precluded by the homogeneous Re atomic distribution in element energy dispersive spectroscopy (EDS) mapping (Figure S10c). Furthermore, X-ray absorption near-edge structure (XANES) spectrum of HOF-25-Re at Re L<sub>3</sub>-edge is similar to that of Re(bpy)(CO)<sub>3</sub>Cl (Figure S14), revealing the monovalent nature of Re involved in this HOF. Fitting of extended X-ray adsorption fine structure (EXAFS) spectroscopic data of HOF-25-Re at Re L<sub>3</sub>-edge was performed on an octahedral coordination geometry of Re<sup>I</sup> atom (Figure 2c), consisting of one chloride anion, three carbonyl C atoms, and two bpy N atoms. The Re-Cl, Re-C, and Re-N distances are fitted as 2.38, 2.10, and 2.01 Å, respectively (Table S1). These distances are consistent with the Re(bpy)(CO)<sub>3</sub>Cl benchmark (Table S1), confirming the covalent graft of Re(bpy)(CO)<sub>3</sub>Cl segments on HOF-25.

### Permanent Porosity Study

Similar to many porous organic crystals reported previously,<sup>[7b,d,h,8]</sup> no nitrogen sorption for activated HOF-25 and HOF-25-Re was determined at 77 K due possibly to the octyl-induced porosity dynamics, which blocks the gas diffusion. The permanent porosities of these two HOFs were evaluated by carbon dioxide sorption at 196 K. The BET surface area of HOF-25 is estimated as 173 m<sup>2</sup>g<sup>-1</sup>. Permanently porous HOF-25 absorbs the CO<sub>2</sub> uptake of 8.3 and 35.5 cm<sup>3</sup>g<sup>-1</sup> under 1 bar at 298 and 273 K, respectively (Figures 2d and S15). After post-modification with Re(CO)<sub>3</sub>Cl segments, the BET surface area of HOF-25-Re is slightly decreased to 149 m<sup>2</sup>g<sup>-1</sup> due to the partly porosity collapse (Figure 2d). Porous architecture of HOF-25-Re is helpful for the absorption and diffusion of CO<sub>2</sub> molecule in solution.

### Photophysical Investigation of HOF-25-Re

Re(bpy)(CO)<sub>3</sub>Cl is one of the most famous homogeneous photocatalyst to drive CO<sub>2</sub> reduction, but the dimerization-driven deactivation limits its practical use.<sup>[3b]</sup> As a result, it is still of significance to enhance their durability and to create high performance photocatalytic derivatives. Before the photocatalysis, the UV-vis diffuse reflectance spectrum of HOF-25-Re was collected with HOF-25 as reference to explore its light absorption scope. For HOF-25, there is a broad absorption with two peaks at 280 and 419 nm

(Figure S16). After the covalent graft of Re(bpy)(CO)<sub>3</sub>Cl units in HOF-25, the UV-vis diffuse reflectance spectrum becomes much broader due possibly to the metal-to-ligand charge transfer (MLCT) and extended delocalization upon metalation involved,<sup>[15]</sup> (Figure S16). The Tauc plot discloses an optical band gap of 2.25 eV (Figure S17). According to the Mott-Schottky curves collected at frequencies of 500, 1000, and 1500 Hz shown in Figure S18, the flat potential is identified as -1.28 V vs. Ag/AgCl using Kubelka-Munk (KM) method. The conduction band (LUMO) and valence band (HOMO) level for HOF-25-Re therefore were calculated as -1.08 and 1.17 eV (vs. NHE), respectively (Figure S19).

The photophysical behaviors of HOF-25-Re and Re(bpy)(CO)<sub>3</sub>Cl as heterogeneous and homogeneous phase, respectively, in CH<sub>3</sub>CN were collected using nanosecond transient absorption (TA) spectra upon the excitation at 420 nm (Figures 3a-c). For the TA spectra of Re(bpy)(CO)<sub>3</sub>Cl, the broad photoinduced absorption bands appear at 420–550 and 600–1000 nm due to the MLCT of rhenium complexes.<sup>[16]</sup> The photo-induced bleach band is not observed due to the ground-state absorption of Re(bpy)(CO)<sub>3</sub>Cl beyond the present testing range (Figure 3a). With respect to the TA spectra of HOF-25-Re in Figure 3b, the photo-induced bleach bands observed before 500 nm are close to the ground-state absorption peak, being assigned to its ground state bleach. An excited state absorption from 600 to 1000 nm for HOF-25-Re is similar to that of Re(bpy)(CO)<sub>3</sub>Cl due to the formation of the excited MLCT state. The normalized single-wavelength dynamics curves of HOF-25-Re and Re(bpy)(CO)<sub>3</sub>Cl probed at 750 nm reveal that the excited state of HOF-25-Re exhibits longer lifetime ( $\tau = 102.8$  ns) than ( $\tau = 31.2$  ns) that of Re(bpy)(CO)<sub>3</sub>Cl (Figure 3c), suggesting the effective role of Re-functionalized HOF in heterogeneous phase in inhibiting charge recombination. These data indicate

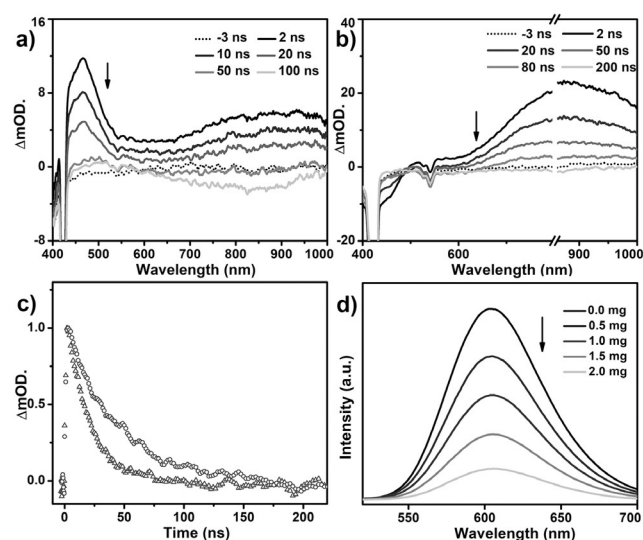


**Figure 3.** Transient adsorption spectra of Re(bpy)(CO)<sub>3</sub>Cl (a) and HOF-25-Re (b) with 420 nm excitation. c) Normalized kinetic traces of the 750 nm band for Re(bpy)(CO)<sub>3</sub>Cl (triangle) and HOF-25-Re (circle). d) Steady state fluorescence spectra of [Ru(bpy)<sub>3</sub>]Cl<sub>2</sub> upon the addition of HOF-25-Re ( $\lambda_{\text{ex}} = 420$  nm).

the much more reaction opportunities between the excited states of HOF catalyst and CO<sub>2</sub>, being favorable for CO<sub>2</sub> reduction.

### Heterogeneous Photocatalysis of HOF-25-Re

Among various photocatalysts for CO<sub>2</sub> reduction, molecular metal complexes have shown prominent superiority in structure tailorability, mechanistic investigation, product selectivity, and price.<sup>[17]</sup> Incorporation of molecular catalysts with porous materials such as MOFs<sup>[1a,3a-c]</sup> and COFs<sup>[4]</sup> effectively heterogenize the homogeneous catalysts for the easy product isolation and catalyst recycle, prolonging their service lives. In this case, HOF-25-Re seems to be a new prototype to elucidate the possibility of heterogenizing molecular catalysts by HOFs for photocatalytic CO<sub>2</sub> reduction. As a consequence, the CO<sub>2</sub> photoreduction performance of 5-minute sonication-treated porous HOF-25-Re (5.0 mg) was tested in the presence of TIPA sacrificial reagent in CH<sub>3</sub>CN with the assistance of bpy (Figure S20). Upon visible-light irradiation (300 W Xe lamp,  $\lambda \geq 420$  nm) and under the CO<sub>2</sub> pressure at 1.0 bar for 2.0 hours, gas chromatography (GC) analysis detects a binary product containing CO and H<sub>2</sub>. The CO evolution amount of 56  $\mu\text{mol g}^{-1}$ . This value is far lower than that (4869  $\mu\text{mol g}^{-1}$ ) for Re(bpy)(CO)<sub>3</sub>Cl homogeneous catalyst (5.0 mg) under the same reaction conditions due to the weaker light absorption capability of HOF-25-Re solid than molecular catalyst in solution. In addition, the strong electron back-donation from Re ion to carbonyl ligand of HOF-25-Re, as the indication of the much higher peak intensity of Re L<sub>3</sub>-edge for this HOF catalyst than Re(bpy)(CO)<sub>3</sub>Cl benchmark (Figure S14), may be adverse to the excitation under the present photocatalytic condition. Prolonging the reaction time to 12.0 hours, the generated CO amount upon HOF-25-Re is slowly increased to 271  $\mu\text{mol g}^{-1}$ . In contrast, the evolved CO amount with Re(bpy)(CO)<sub>3</sub>Cl is constant from 2.0 to 12.0 hours due possibly to the dimerization-driven deactivation. During the photocatalysis proceeding in 12.0 hours, TON (4.8) of HOF-25-Re finally surpasses that of homogeneous control (2.2), because the covalent attachment of Re(bpy)(CO)<sub>3</sub>Cl on porous HOF precludes the dimerization-driven deactivation of molecular photocatalysts.

With the addition of [Ru(bpy)<sub>3</sub>]Cl<sub>2</sub>·6H<sub>2</sub>O into the above photocatalytic system and the irradiation of 2.0 hours, the CO and H<sub>2</sub> evolution rates are significantly increased to 1448 and 108  $\mu\text{mol g}^{-1} \text{h}^{-1}$ , respectively (Figure 4a). In particular for CO evolution rate, it was enhanced 51 times in comparison with that (28  $\mu\text{mol g}^{-1} \text{h}^{-1}$ ) in the absence of photosensitizer due to the introduction of electron transfer from [Ru(bpy)<sub>3</sub>]Cl<sub>2</sub> to HOF-25-Re.<sup>[15,18]</sup> In the control experiment by reducing the amount of HOF-25-Re (2.0 mg), the highly selective photocatalytic performance, in term of the CO evolution rates of 3030  $\mu\text{mol g}^{-1} \text{h}^{-1}$ , is much superior to that of photocatalyst (5.0 mg) (Table 1). Such a rapid CO evolution rate and high product selectivity of 93% obviously surpass those excellent photocatalysts such as Ni-TpBpy,<sup>[4a]</sup> MAF-X27-OH,<sup>[19]</sup> and MOF-Co<sup>[20]</sup> under the help of [Ru(bpy)<sub>3</sub>]Cl<sub>2</sub>·6H<sub>2</sub>O photosensitizer (Table 1). The TON (50.4)

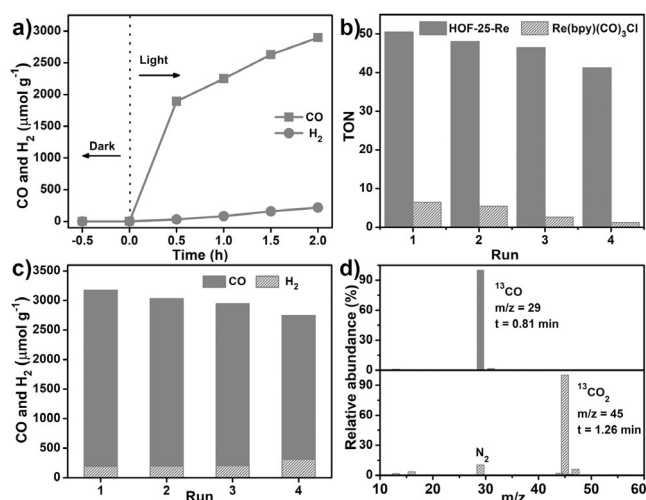


**Figure 4.** a) Time-dependent CO and H<sub>2</sub> evolution for the visible-light irradiated photocatalytic system with HOF-25-Re and CO<sub>2</sub> at 1.0 bar in presence of [Ru(bpy)<sub>3</sub>]Cl<sub>2</sub>·6H<sub>2</sub>O and TIPA in CH<sub>3</sub>CN. b) The TON comparison of the CO<sub>2</sub> photoreduction between HOF-25-Re and Re(bpy)(CO)<sub>3</sub>Cl in heterogeneous and homogeneous phase, respectively. c) Stability test of HOF-25-Re photocatalyst with 2.0 h each run. d) Mass spectrum of <sup>13</sup>CO produced from the photocatalytic reduction of <sup>13</sup>CO<sub>2</sub>.

**Table 1:** Comparison of Reported Catalysts for Photocatalytic CO<sub>2</sub> Reduction to CO with the Help of [Ru(bpy)<sub>3</sub>]Cl<sub>2</sub> Photosensitizer under Visible Light Irradiation in 1.0 atm CO<sub>2</sub>.

Catalyst	Rate of CO [ $\mu\text{mol g}^{-1} \text{h}^{-1}$ ]	Selectivity of CO [%]	Ref.
HOF-25-Re <sup>[a]</sup>	1448	93	this work
HOF-25-Re <sup>[b]</sup>	3030	92	this work
Ni-TpBpy	966	96	[4a]
MAF-X27-OH	225.8	97	[19]
MOF-Co	1140	47	[20]
BIF-29	3334	83	[21]
Co <sub>3</sub> O <sub>4</sub> platelets	2003	77	[22]
Re-Bpy-sp <sup>2</sup> c-COF	1400	86	[23]
PI-COF-TT	483	93	[24]
COF-367-Co NSs	10162	78	[25]

[a] HOF-25-Re (5.0 mg). [b] HOF-25-Re (2.0 mg).

based on Re atoms is about eight times than that (6.3) of homogeneous control Re(bpy)(CO)<sub>3</sub>Cl at the same reaction condition (Figure 4b). In contrast, there is only a little amount of CO detected in the blank, non-photosensitizer, non-sacrificial reagent, non-irradiation, HOF-25, and N<sub>2</sub> control experiments (Figure S21), suggesting the Re(bpy)(CO)<sub>3</sub>Cl units in HOF-25-Re serve as catalytically active sites for the present photocatalysis of CO<sub>2</sub> reduction. The high CO/H<sub>2</sub> selectivity of HOF-25-Re (93%) is the same as that of the homogeneous molecular counterpart Re(bpy)(CO)<sub>3</sub>Cl. In particular, after the photo-driven conversion of CO<sub>2</sub> to CO, about 3.4% Re content in HOF-25-Re was determined to be leached into the filtrate on the basis of the ICP data, suggesting the moderate stability of Re(bpy)(CO)<sub>3</sub>Cl unit in this HOF material. The high CO evolution rate above 1350  $\mu\text{mol g}^{-1} \text{h}^{-1}$  and 93% product selectivity for heteroge-

neous HOF-25-Re photocatalyst are able to be lasted for three cycles (Figure 4c). Photocatalytic CO<sub>2</sub>-to-CO conversion upon HOF-25-Re for 16.0 hours (8 cycles) deactivated this catalyst, giving a low CO generation rate of 784 μmol g<sup>-1</sup> h<sup>-1</sup> and 68 % selectivity. Self-assembly of L in used HOF-25-Re enables the regeneration of HOF-25, and further post-functionalization with Re centers can recover the catalyst performance with the CO evolution rate of 1671 μmol g<sup>-1</sup> h<sup>-1</sup> and 92 % selectivity (Figures S22 and S23), indicating the sustainable advantage of HOF platform to position molecular catalysts.

### Photocatalysis Mechanism

During the photocatalysis, an electron transfer mechanism from excited [Ru(bpy)<sub>3</sub>]Cl<sub>2</sub>·6H<sub>2</sub>O photosensitizer to HOF-25-Re is suggested by their matched energy levels (Figure S19).<sup>[18b,20]</sup> This point was further probed by the luminescent quenching experiment by adding the HOF-25-Re to a CH<sub>3</sub>CN solution of [Ru(bpy)<sub>3</sub>]Cl<sub>2</sub>·6H<sub>2</sub>O and TIPA.<sup>[21]</sup> The emission at 605 nm is assigned to the metal ligand charge transfer (MLCT) excited state of [Ru(bpy)<sub>3</sub>]Cl<sub>2</sub> (Figure 3d), and the intensity is continuously reduced following the increased amount of HOF-25-Re, implying the occurrence of electron transfer from the excited state of photosensitizer to generate a reduced state of HOF-25-Re.<sup>[18b,26]</sup> In addition, the fitting of luminescent decay profile gives a lifetime (161.3 ns) for photosensitizer (Figure S24). The addition of HOF-25-Re to [Ru(bpy)<sub>3</sub>]Cl<sub>2</sub> solution reduces the lifetime of photosensitizer to 41.7 ns. Such shortened luminescent lifetime also suggests that photo-induced electrons transfer occurs between [Ru(bpy)<sub>3</sub>]Cl<sub>2</sub> and HOF-25-Re to trigger the photocatalysis. Actually, the electron transfer from Ru photosensitizer to Re photocatalyst in the present case is well supported by the excellent photocatalytic systems containing [Ru(bpy)<sub>3</sub>]<sup>+</sup> and Re(bpy)(CO)<sub>3</sub>Cl components revealed previously.<sup>[15,18a]</sup>

After the photocatalysis, <sup>1</sup>H NMR spectroscopic analysis discloses that there is not carbon-containing byproduct in the reaction liquid and the building block of HOF-25 (Figure S25), further indicating the high CO evolution selectivity associated with the heterogeneous HOF catalyst. In addition, powder XRD study reveals the porous periodic structure for the used HOF-25-Re (Figure S26). The photocatalytic performance of the reaction filtrate exhibits the very low and similar CO evolution rate to that of the [Ru(bpy)<sub>3</sub>]Cl<sub>2</sub>·6H<sub>2</sub>O photosensitizer control (Figure S21), precluding the origination of the present photocatalytic behavior from the dissolved HOF-based catalyst. To pursue the carbon source in CO product, gas chromatography and mass spectroscopic study were performed on the outputting gas product evolved from an isotopic <sup>13</sup>CO<sub>2</sub> experiment. A signal of <sup>13</sup>C-labeled CO is observed at *m/z* = 29 (Figures 4d and S27), confirming the present CO<sub>2</sub>-to-CO conversion mechanism.

### Conclusion

In summary, a robust porous biological HOF with the bpy dock group to precisely load molecular catalyst has been designed and prepared on the basis of rigid hydrogen-bonded and π-π stacking metal-free G-quadruplex moieties. With the help of sensitizer, the covalent graft of molecular photocatalyst on this porous HOF promotes efficient and selective CO<sub>2</sub>-to-CO conversion in heterogeneous system. In particular, stable and recyclable HOFs were suggested as a prominent platform in lastingly heterogenizing molecular catalysts. These results not only illustrate a new strategy to construct robust HOFs but also give a clear insight into porous HOF to heterogenize molecular catalysts for carbon dioxide photo-reduction. The present investigation opens a new avenue for engineering functional HOFs by synergistic molecular design and post-modification.

### Acknowledgements

Financial support from the National Natural Science Foundation of China (Nos. 21631003, 21805005, and 22011540002), the Fundamental Research Funds for the Central Universities (No. FRF-BD-20-14A and FRF-IDRY-19-028), University of Science and Technology Beijing is gratefully acknowledged. We are also very grateful for the help and discussion from the groups of Profs. Xianran Xing, Jiemin Liu, and Ichiro Hisaki.

### Conflict of interest

The authors declare no conflict of interest.

**Keywords:** carbon dioxide reduction · heterogeneous catalysis · hydrogen-bonded organic frameworks · post-modification · visible-light photocatalysis

- [1] a) M. Ding, R. W. Flaig, H.-L. Jiang, O. M. Yaghi, *Chem. Soc. Rev.* **2019**, *48*, 2783–2828; b) S. Lin, C. S. Diercks, Y. B. Zhang, N. Kornienko, E. M. Nichols, Y. B. Zhao, A. R. Paris, D. Kim, P. Yang, O. M. Yaghi, C. J. Chang, *Science* **2015**, *349*, 1208–1213; c) W. H. Wang, Y. Himeda, J. T. Muckerman, G. F. Manbeck, E. Fujita, *Chem. Rev.* **2015**, *115*, 12936–12973.
- [2] a) H. Yamashita, K. Mori, Y. Kuwahara, T. Kamegawa, M. Wen, P. Verma, M. Che, *Chem. Soc. Rev.* **2018**, *47*, 8072–8096; b) M. Aresta, A. Dibenedetto, A. Angelini, *Chem. Rev.* **2014**, *114*, 1709–1742.
- [3] a) Y. Bai, Y. Dou, L.-H. Xie, W. Rutledge, J.-R. Li, H. C. Zhou, *Chem. Soc. Rev.* **2016**, *45*, 2327–2367; b) K. M. Choi, D. Kim, B. Rungtaweevoranit, C. A. Trickett, J. T. Barmanbek, A. S. Alshammari, P. Yang, O. M. Yaghi, *J. Am. Chem. Soc.* **2017**, *139*, 356–362; c) G. Lan, Z. Li, S. S. Veroneau, Y. Y. Zhu, Z. Xu, C. Wang, W. Lin, *J. Am. Chem. Soc.* **2018**, *140*, 12369–12373; d) Z.-B. Fang, T.-T. Liu, J. Liu, S. Jin, X.-P. Wu, X.-Q. Gong, K. Wang, Q. Yin, T.-F. Liu, R. Cao, H.-C. Zhou, *J. Am. Chem. Soc.* **2020**, *142*, 12515–12523; e) W.-G. Cui, G.-Y. Zhang, T.-L. Hu, X.-H. Bu, *Coord. Chem. Rev.* **2019**, *387*, 79–120; f) Y.-N. Gong, W. Zhong, Y. Li, Y. Qiu, L. Zheng, J. Jiang, H.-L. Jiang, *J. Am. Chem. Soc.* **2020**, *142*, 16723–16731; g) D. Li, M. Kassymova, X. Cai, S.-Q. Zang, H.-L. Jiang, *Coord. Chem. Rev.* **2020**, *412*,

- 213262–213277; h) H.-Q. Xu, J. Hu, D. Wang, Z. Li, Q. Zhang, Y. Luo, S.-H. Yu, H.-L. Jiang, *J. Am. Chem. Soc.* **2015**, *137*, 13440–13443.
- [4] a) W. Zhong, R. Sa, L. Li, Y. He, L. Li, J. Bi, Z. Zhuang, Y. Yu, Z. Zou, *J. Am. Chem. Soc.* **2019**, *141*, 7615–7621; b) S. Yang, W. Hu, X. Zhang, P. He, B. Pattengale, C. Liu, M. Cendejas, I. Hermans, X. Zhang, J. Zhang, J. Huang, *J. Am. Chem. Soc.* **2018**, *140*, 14614–14618; c) M. Lu, J. Liu, Q. Li, M. Zhang, M. Liu, J. L. Wang, D. Q. Yuan, Y. Q. Lan, *Angew. Chem. Int. Ed.* **2019**, *58*, 12392–12397; *Angew. Chem.* **2019**, *131*, 12522–12527.
- [5] a) R.-B. Lin, Y. He, P. Li, H. Wang, W. Zhou, B. Chen, *Chem. Soc. Rev.* **2019**, *48*, 1362–1389; b) R. M. Barrer, V. H. Shanson, *J. Chem. Soc. Chem. Commun.* **1976**, 333–334; c) G. O. Lloyd, M. W. Bredenkamp, L. J. Barbour, *Chem. Commun.* **2005**, 4053–4055; d) N. B. McKeown, *J. Mater. Chem.* **2010**, *20*, 10588–10597; e) I. Hisaki, C. Xin, K. Takahashi, T. Nakamura, *Angew. Chem. Int. Ed.* **2019**, *58*, 11160–11170; *Angew. Chem.* **2019**, *131*, 11278–11288; f) T. Adachi, M. D. Ward, *Acc. Chem. Res.* **2016**, *49*, 2669–2679; g) P. Brunet, M. Simard, J. D. Wuest, *J. Am. Chem. Soc.* **1997**, *119*, 2737–2738; h) S. A. Dalrymple, G. K. H. Shimizu, *J. Am. Chem. Soc.* **2007**, *129*, 12114–12116; i) B. Wang, R.-B. Lin, Z. Zhang, S. Xiang, B. Chen, *J. Am. Chem. Soc.* **2020**, *142*, 14399–14416.
- [6] a) F. Hu, C. Liu, M. Wu, J. Pang, F. Jiang, D. Yuan, M. Hong, *Angew. Chem. Int. Ed.* **2017**, *56*, 2101–2104; *Angew. Chem.* **2017**, *129*, 2133–2136; b) A. Pulido, L. Chen, T. Kaczorowski, D. Holden, M. A. Little, S. Y. Chong, B. J. Slater, D. P. McMahon, B. Bonillo, C. J. Stackhouse, A. Stephenson, C. M. Kane, R. Clowes, T. Hasell, A. I. Cooper, G. M. Day, *Nature* **2017**, *543*, 657–664; c) M. Mastalerz, I. M. Oppel, *Angew. Chem. Int. Ed.* **2012**, *51*, 5252–5255; *Angew. Chem.* **2012**, *124*, 5345–5348.
- [7] a) Y. Wang, X. Hou, C. Liu, M. K. Albolqany, Y. Wang, N. Wu, C. Chen, B. Liu, *Nat. Commun.* **2020**, *11*, 3124; b) X.-Z. Luo, X.-J. Jia, J.-H. Deng, J.-L. Zhong, H.-J. Liu, K.-J. Wang, D.-C. Zhong, *J. Am. Chem. Soc.* **2013**, *135*, 11684–11687; c) H. Wang, B. Li, H. Wu, T.-L. Hu, Z. Yao, W. Zhou, S. Xiang, B. Chen, *J. Am. Chem. Soc.* **2015**, *137*, 9963–9970; d) Z. Bao, D. Xie, G. Chang, H. Wu, L. Li, W. Zhou, H. Wang, Z. Zhang, H. Xing, Q. Yang, M. J. Zaworotko, Q. Ren, B. Chen, *J. Am. Chem. Soc.* **2018**, *140*, 4596–4603; e) T.-H. Chen, I. Popov, W. Kaveevivitchai, Y.-C. Chuang, Y.-S. Chen, O. Daugulis, A. J. Jacobson, O. S. Miljanic, *Nat. Commun.* **2014**, *5*, 5131; f) I. Brekalo, D. E. Deliz, L. J. Barbour, M. D. Ward, T. Friscic, K. T. Holman, *Angew. Chem. Int. Ed.* **2020**, *59*, 1997–2002; *Angew. Chem.* **2020**, *132*, 2013–2018; g) S. Feng, Y. Shang, Z. Wang, Z. Kang, R. Wang, J. Jiang, L. Fan, W. Fan, Z. Liu, G. Kong, Y. Feng, S. Hu, H. Guo, D. Sun, *Angew. Chem. Int. Ed.* **2020**, *59*, 3840–3845; *Angew. Chem.* **2020**, *132*, 3868–3873; h) Y. He, S. Xiang, B. Chen, *J. Am. Chem. Soc.* **2011**, *133*, 14570–14573.
- [8] P. Li, Y. He, J. Guang, L. Weng, J. C. Zhao, S. Xiang, B. Chen, *J. Am. Chem. Soc.* **2014**, *136*, 547–549.
- [9] a) Y. Wang, D. Liu, J. Yin, Y. Shang, J. Du, Z. Kang, R. Wang, Y. Chen, D. Sun, J. Jiang, *Chem. Commun.* **2020**, *56*, 703–706; b) B. Wang, R. He, L. H. Xie, Z. J. Lin, X. Zhang, J. Wang, H. Huang, Z. Zhang, K. S. Schanze, J. Zhang, S. Xiang, B. Chen, *J. Am. Chem. Soc.* **2020**, *142*, 12478–12485; c) H. Wang, Z. Bao, H. Wu, R. B. Lin, W. Zhou, T. L. Hu, B. Li, J. C. Zhao, B. Chen, *Chem. Commun.* **2017**, *53*, 11150–11153.
- [10] a) B. Han, H. Wang, C. Wang, H. Wu, W. Zhou, B. Chen, J. Jiang, *J. Am. Chem. Soc.* **2019**, *141*, 8737–8740; b) W. Gong, D. Chu, H. Jiang, X. Chen, Y. Cui, Y. Liu, *Nat. Commun.* **2019**, *10*, 600.
- [11] a) G. Xing, T. Yan, S. Das, T. Ben, S. Qiu, *Angew. Chem. Int. Ed.* **2018**, *57*, 5345–5349; *Angew. Chem.* **2018**, *130*, 5443–5447; b) A. Karmakar, R. Illathvalappil, B. Anothumakkool, A. Sen, P. Samanta, A. V. Desai, S. Kurungot, S. K. Ghosh, *Angew. Chem. Int. Ed.* **2016**, *55*, 10667–10671; *Angew. Chem.* **2016**, *128*, 10825–10829; c) Y. Wang, M. Zhang, Q. Yang, J. Yin, D. Liu, Y. Shang, Z. Kang, R. Wang, D. Sun, J. Jiang, *Chem. Commun.* **2020**, *56*, 15529–15532.
- [12] a) Q. Yin, P. Zhao, R.-J. Sa, G.-C. Chen, J. Lu, T.-F. Liu, R. Cao, *Angew. Chem. Int. Ed.* **2018**, *57*, 7691–7696; *Angew. Chem.* **2018**, *130*, 7817–7822; b) X. Zhang, L. Li, J.-X. Wang, H.-M. Wen, R. Krishna, H. Wu, W. Zhou, Z.-N. Chen, B. Li, G. Qian, B. Chen, *J. Am. Chem. Soc.* **2020**, *142*, 633–640; c) I. Hisaki, Y. Suzuki, E. Gomez, Q. Ji, N. Tohnai, T. Nakamura, A. Douhal, *J. Am. Chem. Soc.* **2019**, *141*, 2111–2121.
- [13] a) Y.-L. Wu, N. E. Horwitz, K.-S. Chen, D. A. Gomez-Gualdrón, N. S. Luu, L. Ma, T. C. Wang, M. C. Hersam, J. T. Hupp, O. K. Farha, R. Q. Snurr, M. R. Wasielewski, *Nat. Chem.* **2017**, *9*, 466–472; b) Y.-L. Wu, N. S. Bobbitt, J. L. Logsdon, N. E. Powers-Riggs, J. N. Nelson, X. Liu, T. C. Wang, R. Q. Snurr, J. T. Hupp, O. K. Farha, M. C. Hersam, M. R. Wasielewski, *Angew. Chem. Int. Ed.* **2018**, *57*, 3985–3989; *Angew. Chem.* **2018**, *130*, 4049–4053; c) N. E. Powers-Riggs, X. Zuo, R. M. Young, M. R. Wasielewski, *J. Am. Chem. Soc.* **2019**, *141*, 17512–17516; d) L. Wu, K. Liu, J. Jie, D. Song, H. Su, *J. Am. Chem. Soc.* **2015**, *137*, 259–266; e) J. T. Davis, G. P. Spada, *Chem. Soc. Rev.* **2007**, *36*, 296–313.
- [14] H.-P. Liang, A. Acharjya, D. A. Anito, S. Vogl, T.-X. Wang, A. Thomas, B.-H. Han, *ACS Catal.* **2019**, *9*, 3959–3968.
- [15] A. M. Cancelliere, F. Puntoriero, S. Serroni, S. Campagna, Y. Tamaki, D. Saito, O. Ishitani, *Chem. Sci.* **2020**, *11*, 1556–1563.
- [16] S. Y. Reece, D. G. Nocera, *J. Am. Chem. Soc.* **2005**, *127*, 9448–9458.
- [17] a) J.-W. Wang, D.-C. Zhong, T.-B. Lu, *Coord. Chem. Rev.* **2018**, *377*, 225–236; b) E. Boutin, L. Merakeb, B. Ma, B. Boudy, M. Wang, J. Bonin, E. Anxolabehere-Mallart, M. Robert, *Chem. Soc. Rev.* **2020**, *49*, 5772–5809; c) L. Chen, G. Chen, C. F. Leung, C. Cometto, M. Robert, T.-C. Lau, *Chem. Soc. Rev.* **2020**, *49*, 7271–7283; d) K. E. Dalle, J. Warnan, J. J. Leung, B. Reuillard, I. S. Karmel, E. Reisner, *Chem. Rev.* **2019**, *119*, 2752–2875.
- [18] a) D. Saito, Y. Yamazaki, Y. Tamaki, O. Ishitani, *J. Am. Chem. Soc.* **2020**, *142*, 19249–19258; b) H.-L. Zheng, S.-L. Huang, M.-B. Luo, Q. Wei, E.-X. Chen, L. He, Q. Lin, *Angew. Chem. Int. Ed.* **2020**, *59*, 23588–23592; *Angew. Chem.* **2020**, *132*, 23794–23798.
- [19] Y. Wang, N.-Y. Huang, J. Q. Shen, P.-Q. Liao, X.-M. Chen, J.-P. Zhang, *J. Am. Chem. Soc.* **2018**, *140*, 38–41.
- [20] X.-K. Wang, J. Liu, L. Zhang, L.-Z. Dong, S.-L. Li, Y.-H. Kan, D.-S. Li, Y.-Q. Lan, *ACS Catal.* **2019**, *9*, 1726–1732.
- [21] H.-X. Zhang, Q.-L. Hong, J. Li, F. Wang, X. Huang, S. Chen, W. Tu, D. Yu, R. Xu, T. Zhou, J. Zhang, *Angew. Chem. Int. Ed.* **2019**, *58*, 11752–11756; *Angew. Chem.* **2019**, *131*, 11878–11882.
- [22] C. Gao, Q. Meng, K. Zhao, H. Yin, D. Wang, J. Guo, S. Zhao, L. Chang, M. He, Q. Li, H. Zhao, X. Huang, Y. Gao, Z. Tang, *Adv. Mater.* **2016**, *28*, 6485–6490.
- [23] Z. Fu, X. Wang, A. M. Gardner, X. Wang, S. Y. Chong, G. Neri, A. J. Cowan, L. Liu, X. Li, A. Vogel, R. Clowes, M. Bilton, L. Chen, R. S. Sprick, A. I. Cooper, *Chem. Sci.* **2020**, *11*, 543–550.
- [24] X. Chen, Q. Dang, R. Sa, L. Li, L. Li, J. Bi, Z. Zhang, J. Long, Y. Yu, Z. Zou, *Chem. Sci.* **2020**, *11*, 6915–6922.
- [25] W. Liu, X. Li, C. Wang, H. Pan, W. Liu, K. Wang, Q. Zeng, R. Wang, J. Jiang, *J. Am. Chem. Soc.* **2019**, *141*, 17431–17440.
- [26] B. Han, X. Ou, Z. Deng, Y. Song, C. Tian, H. Deng, Y. J. Xu, Z. Lin, *Angew. Chem. Int. Ed.* **2018**, *57*, 16811–16815; *Angew. Chem.* **2018**, *130*, 17053–17057.

Manuscript received: December 16, 2020

Revised manuscript received: January 22, 2021

Accepted manuscript online: January 25, 2021

Version of record online: March 9, 2021